ACS Photonics
Letter
pubs.acs.org/journal/apchd5

Second-Harmonic Generation from Critically Coupled Surface Phonon Polaritons

Nikolai Christian Passler, Ilya Razdolski, Sandy Gewinner, Wieland Schöllkopf, Martin Wolf, and Alexander Paarmann*

Fritz-Haber-Institut der Max-Planck-Gesellschaft, Faradayweg 4-6, 14195 Berlin, Germany

Supporting Information

ABSTRACT: Mid-infrared nanophotonics can be realized using subdiffractional light localization and field enhancement with surface phonon polaritons in polar dielectric materials. We experimentally demonstrate second-harmonic generation due to the optical field enhancement from critically coupled surface phonon polaritons at the 6H-SiC−air interface, employing an infrared free-electron laser for intense, tunable, and narrowband mid-infrared excitation. Critical coupling to the surface polaritons is achieved using a prism in the Otto geometry with adjustable width of the air gap, providing a contact-free access to the polariton dispersion with full control over the excitation conditions. The calculated reflectivity and second-harmonic spectra reproduce the complete experimental data set with high accuracy, allowing for a quantification of the optical field enhancement. We also reveal the mechanism for low out-coupling efficiency of the second-harmonic light in the Otto geometry. Perspectives on surface phonon polariton-based nonlinear sensing and nonlinear waveguide coupling are discussed.

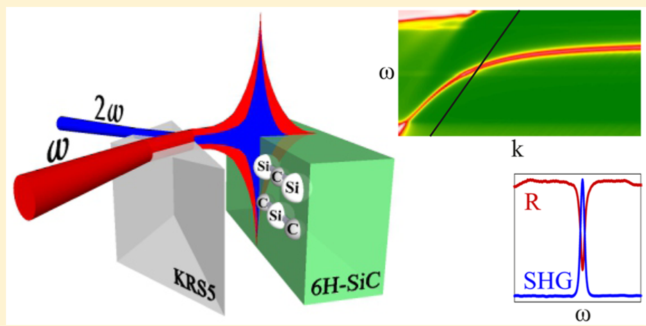

KEYWORDS: *surface phonon polariton, Otto geometry, nonlinear optics, silicon carbide, nanophononics, infrared free-electron laser*

Surface polaritons are the key building block of nanophotonics since these excitations allow for extreme light localization accompanied by significant enhancement of the local optical fields. A large body of research has focused on surface plasmon polaritons (SPPs) at noble metal surfaces,[1] which has led to a number of applications ranging from optical near-field microscopy to nonlinear plasmonic nanosensors.[2−7] Recently, an alternative approach was introduced employing surface phonon polaritons (SPhPs), which can be excited in the mid-infrared (mid-IR) at the surface of polar dielectrics.[8−10] In these materials, optical phonon resonances in the dielectric response result in a negative permittivity in the Reststrahl range between the transverse optical (TO) and longitudinal optical (LO) phonon frequencies and, in consequence, the existence of a highly dispersive surface polariton.[11] Notably, the much reduced optical losses of SPhPs as compared to SPPs have been argued to potentially solve the loss problem that was identified as the key limitation for widespread implementation of plasmonic devices.[12,13] Recent pioneering experiments have employed SPhPs for optical switching,[14] as well as subdiffractional light confinement[15−17] and strongly enhanced nonlinear response in subwavelength nanostructures.[18]

A systematic study of the linear and nonlinear-optical response of surface polaritons is enabled by prism coupling either in Kretschmann−Raether[19] or Otto[20] configuration. In both cases, the high refractive index of the prism operated in a regime of total internal reflection provides the large momenta required to excite the surface waves.[19] While mostly employed for studies of SPPs,[21−25] a few works also investigated SPhPs with prism coupling in the mid-IR.[8,10,26,27] Specifically in the Otto configuration, the surface polariton is excited across an air gap of adjustable width, providing contact-free access to the surface mode with extrinsic tunability of the excitation efficiency, which can lead to critical coupling conditions.[10] Strong optical field enhancement at critical coupling was predicted but could not be experimentally confirmed using linear optical techniques. Instead, nonlinear-optical approaches such as second-harmonic generation (SHG) are highly sensitive to the localized electromagnetic fields.[18,22,25,28−30]

In this Letter, we experimentally demonstrate the first SHG from critically coupled SPhPs, allowing us to accurately determine the associated optical field enhancement. We employ the Otto geometry for prism coupling to SPhPs at the 6H-SiC−air interface across a variable air gap and detect reflectivity and SHG output spectroscopically at various positions in the SPhP dispersion, using an infrared free-electron laser (FEL) for tunable narrowband excitation. By varying the air gap width between the prism and the sample, we demonstrate critical coupling behavior of the SPhP excitation efficiency. The calculated linear and nonlinear response reproduces the full data set of reflectivity and SHG spectra with high accuracy. We

Received: February 7, 2017
Published: April 11, 2017

DOI: 10.1021/acsphotonics.7b00118
ACS Photonics 2017, 4, 1048−1053

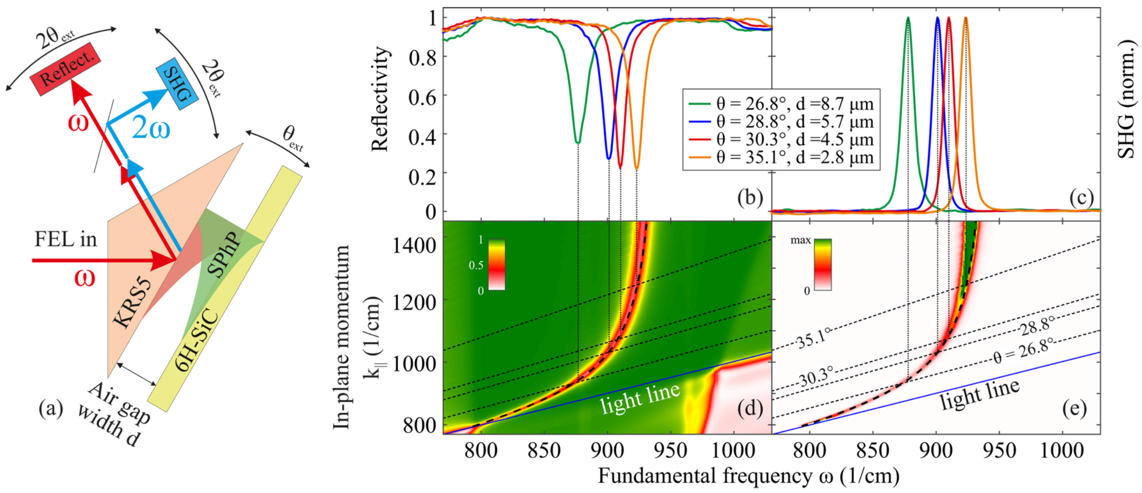

Figure 1. (a) Schematic of the experimental setup (not to scale) for Otto-type prism coupling to propagating SPhPs. Tuning the FEL frequency ω, air gap width d, and excitation-detection angle θ_{ext}−$2\theta_{ext}$ allows for full control over the SPhP excitation conditions. We measure both SHG intensity and reflectivity of the fundamental beam simultaneously using a dichroic beam splitter. For illustration, we also schematically show the evanescent fields leaking into the air gap from the prism side (red shaded) and SPhP (green shaded) at critical coupling conditions. Experimental reflectivity (b) and SHG (c) spectra taken for multiple incidence angles, each near the respective critical coupling gap width (see legend), leading to the most efficient SPhP excitation. Calculated reflectivity (d) and SHG (e) maps evaluated at critical coupling conditions show how the signals follow the SPhP dispersion (thick dashed lines): for each given incidence angle θ, the in-plane momentum of the fundamental light (sloped dashed lines) intersects with the SPhP dispersion at the respective spectral positions of the SPhP resonances in the reflectivity and SHG (vertical dotted lines).

extract the optical field enhancement, analyze the out-coupling of the SHG intensity in the Otto geometry, and discuss several potential applications of the nonlinear response from SPhPs.

■ RESULTS AND DISCUSSION

Excitation of propagating SPhPs and detection of their reflectivity and SHG response is realized experimentally as schematically shown in Figure 1a. We implement the Otto arrangement[8,10,20] by placing a triangular prism (KRS5, $n_{prism} \approx 2.4$, Korth) operated in the regime of total internal reflection onto a motorized mount in front of the sample, allowing for continuous tuning of the air gap width d. Rotation of the prism−sample assembly by angle $\Delta\theta_{ext} \approx n_{prism}\Delta\theta$ changes the in-plane momentum $k_{\parallel} = \frac{\omega}{c} n_{prism} \sin\theta$ of the incoming wave, allowing to excite SPhPs at different points along the dispersion.[8] Here, θ is the incidence angle inside the prism of refractive index n_{prism}, and ω is the frequency of the incoming mid-IR beam. We use an infrared FEL[31] as tunable, narrow band p-polarized excitation source, and the reflected fundamental and SHG beams are detected after a dichroic beam splitter. As a sample, we use a semi-insulating 6H-SiC c-cut single crystal; see the Supporting Information for further details on the experiment.

Notably, the efficiency of coupling the incoming light to the SPhPs in this geometry sensitively depends on the air gap width d.[10] The decay length L of the evanescent waves into the air gap for both the totally reflected incoming light and the SPhP strongly varies with the in-plane momentum $k_{\parallel}$:[19]

$$L = \frac{\lambda}{2\pi\sqrt{k_{\parallel}^{2}c^{2}/\omega^{2} - 1}} \tag{1}$$

where λ is the wavelength and c the speed of light in a vacuum. For small gaps $d \ll L$ with large overlap of the two evanescent waves, the strong radiative coupling of the SPhP back into the prism is a significant loss channel and prevents efficient excitation, while for large gaps $d \gg L$ the small overlap between the two evanescent waves inhibits an efficient energy transfer. There is, however, a critical coupling gap width d_{crit} where the radiative and intrinsic losses of the SPhP exactly balance each other, and critical coupling to SPhPs is achieved.[10] This is illustrated with the red- and green-shaded areas in Figure 1a for prism-side and SPhP waves, respectively. Since $k_{\parallel}$ strongly varies along the SPhP dispersion, both L and the critical gap width d_{crit} also vary from less than 1 μm for large momenta to tens of μm at small momenta when approaching the light line.

In consequence, the Otto arrangement allows for a high-precision, direct measurement of the full surface polariton dispersion if the critical coupling conditions are adapted appropriately. This mapping of the SPhP dispersion is demonstrated in Figure 1b and c, where we show experimental reflectivity and SHG spectra, respectively, at four different incidence angles, each taken near the respective d_{crit}. Under these conditions, a reflectivity dip of ~80% indicates efficient excitation of the SPhP. The spectral position of the dip follows the SPhP dispersion (see Figure 1d) as the incidence angle is changed. At the same time, the field enhancement associated with the efficiently excited SPhP results in significant increase of the SHG yield, as evidenced by the single, narrow peak in each of the SHG spectra (c).

For comparison, we show calculated reflectivity and SHG maps at critical coupling conditions in Figure 1d and e, respectively, plotted as a function of fundamental frequency ω and in-plane momentum $k_{\parallel}$. The reflectivity is calculated using the transfer matrix approach[32−34] (see Supporting Information for details), while the SHG intensity is computed using

$$I(2\omega) \propto |(T_b \vec{E}_{SiC}(2\omega))(\chi^{(2)}(-2\omega; \omega, \omega)\vec{E}_{SiC}^{\,2}(\omega)/\Delta k)|^2 \tag{2}$$

Here, $\vec{E}_{SiC}(\omega)$ is the local optical field on the SiC side of the SiC−air interface, which we obtain from the transfer matrix approach, and $\chi^{(2)}$ is the nonlinear susceptibility of 6H-SiC,[30] while Δk accounts for the wave vector mismatch for SHG in reflection.[30,35] Additionally, we explicitly account for the field

DOI: 10.1021/acsphotonics.7b00118
ACS Photonics 2017, 4, 1048−1053

coupling of the nonlinear polarization by projecting it onto $T_b\vec{E}_{SiC}(2\omega)$, with $\vec{E}_{SiC}(2\omega)$ being the local field of the respective mode at 2ω and $2k_{\parallel}$ propagating from SiC back into the prism and T_b the transmission coefficient back to the prism. See the Supporting Information for details on the SHG calculations.

To demonstrate the critical behavior of the response, we acquired reflectivity spectra for multiple values of the air gap width d for selected incidence angles, exemplified for $\theta = 28.8°$ and $\theta = 35.1°$ in Figure 2a and b, respectively. At the smallest gap (black lines), a shallow broad dip in the reflectivity at $\omega \approx 900$ cm^{-1} reports on excitation of highly lossy SPhPs with pronounced radiative coupling. As d is increased, the reflectivity dip increases in amplitude and narrows while simultaneously blue-shifting. A maximum dip depth of ~80% (blue lines) indicates that the critical coupling conditions are reached. For even larger gaps (orange lines), the amplitude of the dip drops again, while the narrowing and blue-shifting of the resonance converge, approaching the intrinsic line width and frequency of the uncoupled surface polariton, cf. Figure 1d. The qualitative behavior is identical between the two incidence angles shown here. However, the respective air gaps are clearly different; see legends in Figure 1a and b, where d essentially scales with the evanescent length L in eq 1. The calculated reflectivity perfectly reproduces the experimental data, including subtle features due to the 6H-SiC crystal anisotropy, such as reflectivity dips at the zone-folded weak modes at ~885 cm^{-1} and the axial LO phonon at 964 cm^{-1}.[30,36,37]

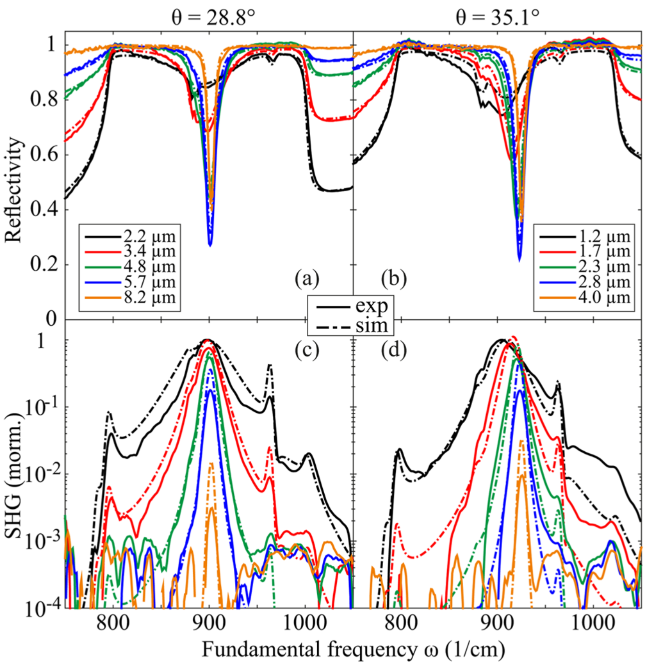

Figure 2. Experimental (solid lines) and calculated (dot-dashed lines) reflectivity (a, b) and SHG (c, d) spectra of the 6H-SiC−air interface in the Otto geometry, shown for selected air gap widths d (see legends) and incidence angles $\theta = 28.8°$ (a, c) and $\theta = 35.1°$ (b, d). The SHG spectra were normalized to the maximum at the smallest gap width. Note the logarithmic scale in (c) and (d).

The simultaneously acquired SHG spectra are shown in Figure 2c,d. At small gaps, the data exhibit some additional spectral features;[30,35] however, a pronounced SPhP resonance can be clearly distinguished (note the logarithmic scale), with SPhP peak positions and line widths qualitatively following those observed in the reflectivity as d is increased. However, the amplitude behavior is clearly different for the SHG; we observe a steady decrease of the SHG amplitude at the SPhP resonance with increasing d. The calculated SHG spectra also shown in Figure 2c,d (dash-dotted lines) not only reproduce all the features in the spectra with high accuracy, but also predict the steady decrease of the SPhP resonance amplitude of the SHG with increasing width d of the air gap. This is very surprising, since the maximum field enhancement and, in consequence, most efficient nonlinear signal generation are expected at critical coupling.[10,19]

We summarize the SPhP resonance behavior for the full experimental data set in Figure 3. Lorentzian fits of the SPhP

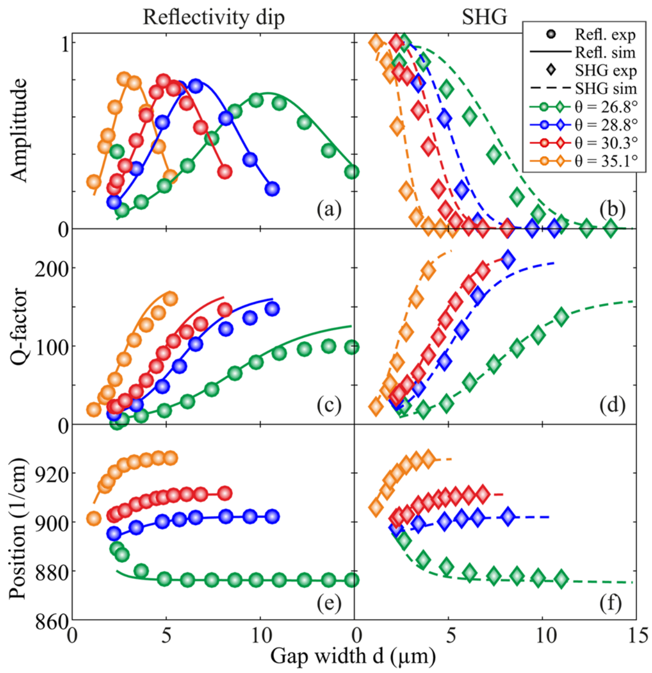

Figure 3. Air gap width d-dependence of the SPhP resonance amplitude (a, b), Q-factor (c, d), and spectral position (e, f) at four different incidence angles, as extracted from the experimental (symbols) and calculated (lines) reflectivity (a, c, e) and SHG (b, d, f) spectra. Critical coupling is achieved at the respective maximum of the reflectivity dip amplitude in (a). The Q-factors increase and the spectral positions shift as d is increased, converging toward the values of the weakly coupled, intrinsic surface polariton resonance, more rapidly with increasing θ and $k_{\parallel}$, i.e., further away from the light line.

resonance in the experimental (symbols) and theoretical (lines) reflectivity (a, c, e) and SHG (b, d, f) spectra yield the amplitude (a, b), Q-factor (c, d), and position (e, f) of the reflectivity dip and SHG peak, respectively. The high experimentally achieved Q-factors, i.e., the ratios between center frequency and line width, mark the high quality of the SPhP resonance. Notably, the SHG resonances are intrinsically narrower as compared to the reflectivity dips due to the second-order nature of the interaction, leading to the consistently higher Q-factors. Remarkable agreement between experiment and theory is observed throughout the full data set. We note here that these calculations use a single set of parameters globally extracted from the full reflectivity data set. Hereby we explicitly include angular beam divergence and finite spectral width of the light source, being the main experimental limitations for achieving full SPhP resonance amplitude near

DOI: 10.1021/acsphotonics.7b00118
ACS Photonics 2017, 4, 1048−1053

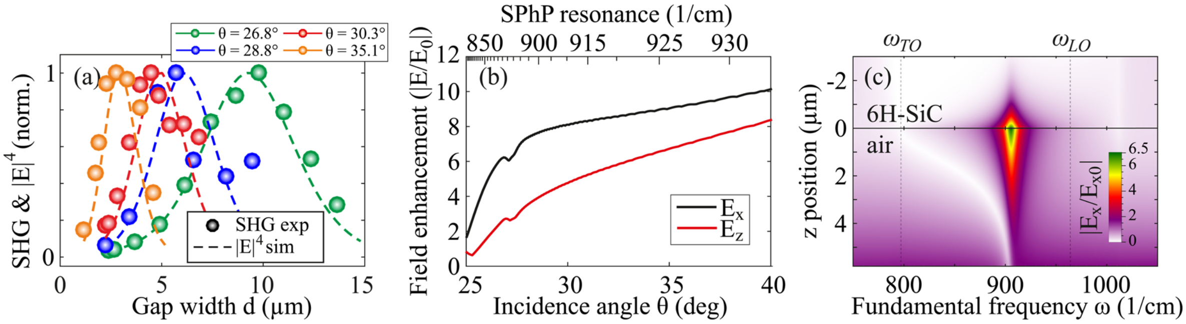

Figure 4. (a) The SHG signals corrected for out-coupling losses (symbols) perfectly follow the fourth power of the calculated local optical fields (lines). (b) SPhP optical field enhancement $|E/E_0|$ with E_0, the incoming field magnitude, evaluated at the critical coupling gap for in-plane E_x (black) and out-of-plane E_z (red) field components as a function of internal incidence angle (bottom) and corresponding SPhP resonance position (top). (c) Example of the spatio-spectral distribution of in-plane field enhancement, shown at critical coupling for $\theta = 28.8°$ with $d = 5.8$ μm. All electric fields are evaluated on the SiC side of the SiC−air interface.

to and far away from the light line, respectively; see the Supporting Information for details. We emphasize that only the reflectivity data were used for the global fitting, while the SHG spectra were simply calculated using nonlinear susceptibility extracted in previous experiments.[30]

The direct comparison of the SPhP resonance amplitudes of the reflectivity dip and the SHG peak (see Figure 3a and b, respectively) for the different incidence angles suggests a correlation between the critical coupling gap marking the strongest modulation of the reflectivity and the apparent decay length of the SHG amplitude. Indeed, if rescaled for the respective critical coupling gap width d_{crit}, the curves for different incidence angles are almost identical; see Figure S3 in the Supporting Information. To understand these observations, we need to consider two mechanisms determining the detectable SHG signal in the far field: (i) efficiency of SHG due to the local field enhancement provided by the SPhPs and (ii) the out-coupling of that nonlinear signal across the air gap into the prism and into the far field. In the case of low losses, the local field enhancement associated with surface polariton excitations is typically expected to follow the magnitude of the reflectivity dip;[10,19] that is, the maximum enhancement should be achieved at the critical coupling condition.

It is, however, important to realize that the SHG is generated with large in-plane momentum $k_{\parallel,SHG} = 2\, k_{SPhP} > k_{0,SHG}$, where $k_{0,SHG}$ is the wavenumber of the SHG light propagating in air. This corresponds to the condition of total internal reflection for the SHG at the SiC−air interface, and only an evanescent wave is expected to leak into the air gap. Evaluating eq 1 for this wave reveals exactly half the evanescent length for the SHG as compared to the fundamental radiation on both sides of the air gap, resulting in an extremely poor overlap and largely suppressed far-field coupling of the SHG at critical coupling conditions. In our SHG calculations, this effect is explicitly accounted for by the gap width d-dependence of $T_b\vec{E}_{SiC}(2\omega)$ in eq 2, whose amplitude rapidly decays with d. In fact, we find that at critical coupling only ~0.1% of the generated nonlinear signal is harvested into the far-field intensity.

Therefore, we can recover the second-harmonic intensity generated in SiC by correcting the experimental signals for the out-coupling efficiency $|T_b\, \vec{E}_{SiC}(2\omega)|^2$, as shown in Figure 4a. As expected from the last factor in eq 2, these signals now follow the fourth power of the resonantly enhanced fundamental optical fields $|E_{SiC}(\omega)|$, which are also plotted there. With this information, we can confidently extract the magnitude of the field enhancement in SiC at critical coupling, which is plotted in Figure 4b along the SPhP dispersion. We plot both in-plane and out-of-plane fields, E_x and E_z, respectively, since due to the symmetry of the $\chi^{(2)}$ tensor, both components contribute significantly to the SHG output.[30] Notably, the small dip in these curves at $\theta \approx 27.5°$ marks the resonant interaction of the SPhP with the zone-folded phonon modes in 6H-SiC.[18] For illustration, we also show an example of the spatio-spectral distribution of field enhancement along the normal-to-surface direction z in Figure 4c.

The excellent agreement between the experimental and calculated SHG response corroborates our observation of the extremely efficient nonlinear-optical conversion inside the SiC crystal, in particular in comparison to SPPs. From our data, we estimate an exceptional nonlinear conversion efficiency exceeding ~10^{-6}, which is a result of (i) the large field enhancement due to the high Q-factor of the SPhP resonance, (ii) the broken inversion symmetry as well as proximity to an ionic resonance of the nonlinear susceptibility[30,38] in the SPhP host, and (iii) the large effective volume of SHG generation as compared for instance to subdiffractional nanostructures.[18]

The broken inversion symmetry and the ionic resonance (ii) are unique fingerprints of SPhP materials as opposed to noble metals used in plasmonics.[1] Hereby, the enhancement of $\chi^{(2)}$ close to the ionic resonance at the TO frequency,[30,38] i.e., in the spectral range where the SPhP can be excited, is a generic feature for all polar dielectrics. Our approach is applicable to all non-centrosymmetric, polar dielectrics, such as α-quartz, ZnO, AlN, InP, GaAs, and ZnTe, to name a few, known to exhibit large nonlinear coefficients, as well as artificially designed hybrid materials[39] with yet unknown SPhP dispersion relations. Additionally, the strong dispersion of SPhPs provides spectral tunability of the field enhancement resonance with extraordinarily high Q-factors.

The combination of these features suggests several appealing scenarios for future applications of nonlinear nanophononics.[18] Previous linear sensing schemes[27,40] could be extended into the nonlinear domain with larger contrasts and higher Q-factors. Taking advantage of the large resonant, high-Q nonlinear signals from the broken-inversion SPhP host, these approaches could straightforwardly be implemented using narrow-bandwidth quantum-cascade lasers. Similarly, our approach could be extended to four-wave mixing experiments,[21,41] sensitive to either the SPhP host or a liquid phase analyte in the gap (cf. Figure 4c for the relevant length scales of field enhancement inside the gap). This could, for instance, lead to a drastic

DOI: 10.1021/acsphotonics.7b00118
ACS Photonics 2017, 4, 1048−1053

resonant enhancement of time-resolved vibrational spectroscopy signals from molecules in solution.[42]

Overall, the Otto geometry provides an ideal platform for studying the linear and nonlinear response from surface polaritons. As compared to the Kretschmann geometry, it allows extrinsically controlling the SPhP coupling efficiency due to the adjustable air gap width and is a contact-free approach that does not require samples to be deposited onto the prism, making it much more versatile. Additionally, we also note that SPhP materials are typically largely transparent above the Reststrahl frequency range. Together with the generation of nonlinear signal under conditions of total internal reflection, this suggests that the Otto geometry could be used for high-contrast nonlinear waveguide coupling,[43] which would also solve the problem of low out-coupling efficiency in reflective SHG detection and allow harvesting the full magnitude of the nonlinear signals.

CONCLUSION

In conclusion, we demonstrated the first SHG from critically coupled SPhPs, enabling high-precision measurements of the associated optical field enhancement, here shown for 6H-SiC as a model system. We use the critical coupling behavior of the Otto geometry to maximize the SPhP excitation efficiency. Despite poor far-field coupling of the SHG signals, which is shown to be a generic feature of the Otto arrangement, the large bulk nonlinearity of the crystal facilitates exceptional nonlinear-optical conversion from SPhPs, owing to the broken inversion symmetry of the host material and the high quality of the SPhP resonance. Being applicable to a wide range of polar dielectrics supporting SPhPs, our approach could be employed to extract the unknown polariton dispersion and field enhancement in artificially designed SPhP hybrids and opens the path to several new and appealing applications of nonlinear nanophononics.

ASSOCIATED CONTENT

Supporting Information

The Supporting Information is available free of charge on the ACS Publications website at DOI: 10.1021/acsphotonics.7b00118.

> Details on the experimental procedure, practical implementation of the Otto geometry and the free-electron laser (S1), details on the transfer matrix calculations (S2), description of the fitting procedure (S3), normalization of the SPhP coupling efficiency data for different incidence angles to the respective critical gap width (S4), and details of the second-harmonic calculations (S5) (PDF)

AUTHOR INFORMATION

Corresponding Author

*E-mail: alexander.paarmann@fhi-berlin.mpg.de.

ORCID

Alexander Paarmann: 0000-0002-8271-2284

Notes

The authors declare no competing financial interest.

ACKNOWLEDGMENTS

The authors thank K. Horn (FHI Berlin) for providing the SiC sample.

REFERENCES

(1) Maier, S. A. *Plasmonics: Fundamentals and Applications*; Springer: US, 2007; pp 1−223.

(2) Sonntag, M. D.; Pozzi, E. A.; Jiang, N.; Hersam, M. C.; Van Duyne, R. P. Recent Advances in Tip-Enhanced Raman Spectroscopy. *J. Phys. Chem. Lett.* **2014**, *5*, 3125−3130.

(3) Müller, M.; Kravtsov, V.; Paarmann, A.; Raschke, M. B.; Ernstorfer, R. Nanofocused Plasmon-Driven Sub-10 fs Electron Point Source. *ACS Photonics* **2016**, *3*, 611−619.

(4) Anker, J. N.; Hall, W. P.; Lyandres, O.; Shah, N. C.; Zhao, J.; Van Duyne, R. P. Biosensing with plasmonic nanosensors. *Nat. Mater.* **2008**, *7*, 442−453.

(5) Kabashin, A. V.; Evans, P.; Pastkovsky, S.; Hendren, W.; Wurtz, G. a.; Atkinson, R.; Pollard, R.; Podolskiy, V. a.; Zayats, a. V. Plasmonic nanorod metamaterials for biosensing. *Nat. Mater.* **2009**, *8*, 867−871.

(6) Martín-Becerra, D.; Armelles, G.; González, M. U.; García-Martín, A. Plasmonic and magnetoplasmonic interferometry for sensing. *New J. Phys.* **2013**, *15*, 085021.

(7) Mesch, M.; Metzger, B.; Hentschel, M.; Giessen, H. Nonlinear Plasmonic Sensing. *Nano Lett.* **2016**, *16*, 3155−3159.

(8) Falge, H. J.; Otto, A. Dispersion of Phonon-Like Surface Polaritons on α-Quartz Observed by Attenuated Total Reflection. *Phys. Status Solidi B* **1973**, *56*, 523−534.

(9) Huber, A. J.; Ocelic, N.; Kazantsev, D.; Hillenbrand, R. Near-field imaging of mid-infrared surface phonon polariton propagation. *Appl. Phys. Lett.* **2005**, *87*, 081103.

(10) Neuner, B.; Korobkin, D.; Fietz, C.; Carole, D.; Ferro, G.; Shvets, G. Critically coupled surface phonon-polariton excitation in silicon carbide. *Opt. Lett.* **2009**, *34*, 2667−9.

(11) Adachi, S. *Optical Properties of Crystalline and Amorphous Semiconductors: Materials and Fundamental Principles*; Springer US: Boston, MA, 1999; pp 33−61.

(12) Khurgin, J. B. How to deal with the loss in plasmonics and metamaterials. *Nat. Nanotechnol.* **2015**, *10*, 2−6.

(13) Caldwell, J. D.; Lindsay, L.; Giannini, V.; Vurgaftman, I.; Reinecke, T. L.; Maier, S. A.; Glembocki, O. J. Low-loss, infrared and terahertz nanophotonics using surface phonon polaritons. *Nanophotonics* **2015**, *4*, 1−26.

(14) Li, P.; Yang, X.; Maß, T. W. W.; Hanss, J.; Lewin, M.; Michel, A.-K. U.; Wuttig, M.; Taubner, T. Reversible optical switching of highly confined phonon-polaritons with an ultrathin phase-change material. *Nat. Mater.* **2016**, *15*, 870−875.

(15) Wang, T.; Li, P.; Hauer, B.; Chigrin, D. N.; Taubner, T. Optical Properties of Single Infrared Resonant Circular Microcavities for Surface Phonon Polaritons. *Nano Lett.* **2013**, *13*, 5051−5055.

(16) Caldwell, J. D.; Glembocki, O. J.; Francescato, Y.; Sharac, N.; Giannini, V.; Bezares, F. J.; Long, J. P.; Owrutsky, J. C.; Vurgaftman, I.; Tischler, J. G.; Wheeler, V. D.; Bassim, N. D.; Shirey, L. M.; Kasica, R.; Maier, S. A. Low-Loss, Extreme Subdiffraction Photon Confinement via Silicon Carbide Localized Surface Phonon Polariton Resonators. *Nano Lett.* **2013**, *13*, 3690−3697.

(17) Gubbin, C. R.; Martini, F.; Politi, A.; Maier, S. A.; De Liberato, S. Strong and Coherent Coupling between Localized and Propagating Phonon Polaritons. *Phys. Rev. Lett.* **2016**, *116*, 246402.

(18) Razdolski, I.; Chen, Y.; Giles, A. J.; Gewinner, S.; Schöllkopf, W.; Hong, M.; Wolf, M.; Giannini, V.; Caldwell, J. D.; Maier, S. A.; Paarmann, A. Resonant Enhancement of Second-Harmonic Generation in the Mid-Infrared Using Localized Surface Phonon Polaritons in Subdiffractional Nanostructures. *Nano Lett.* **2016**, *16*, 6954−6959.

(19) Raether, H. *Surface Plasmons on Smooth and Rough Surfaces and on Gratings*; Springer, 1988.

(20) Otto, A. Excitation of nonradiative surface plasma waves in silver by the method of frustrated total reflection. *Z. Phys. A: Hadrons Nucl.* **1968**, *216*, 398−410.

(21) Palomba, S.; Novotny, L. Nonlinear Excitation of Surface Plasmon Polaritons by Four-Wave Mixing. *Phys. Rev. Lett.* **2008**, *101*, 056802.

DOI: 10.1021/acsphotonics.7b00118
ACS Photonics 2017, 4, 1048−1053

(22) Grosse, N. B.; Heckmann, J.; Woggon, U. Nonlinear Plasmon-Photon Interaction Resolved by k-Space Spectroscopy. *Phys. Rev. Lett.* **2012**, *108*, 136802.
(23) Temnov, V. V. Ultrafast acousto-magneto-plasmonics. *Nat. Photonics* **2012**, *6*, 728−736.
(24) Foley, J. J., IV; Harutyunyan, H.; Rosenmann, D.; Divan, R.; Wiederrecht, G. P.; Gray, S. K. When are Surface Plasmon Polaritons Excited in the Kretschmann-Raether Configuration? *Sci. Rep.* **2015**, *5*, 9929.
(25) Razdolski, I.; Makarov, D.; Schmidt, O. G.; Kirilyuk, A.; Rasing, T.; Temnov, V. V. Nonlinear Surface Magnetoplasmonics in Kretschmann Multilayers. *ACS Photonics* **2016**, *3*, 179−183.
(26) Okada, T.; Nagai, M.; Tanaka, K. Resonant phase jump with enhanced electric field caused by surface phonon polariton in terahertz region. *Opt. Express* **2008**, *16*, 5633.
(27) Zheng, G.; Xu, L.; Zou, X.; Liu, Y. Excitation of surface phonon polariton modes in gold gratings with silicon carbide substrate and their potential sensing applications. *Appl. Surf. Sci.* **2017**, *396*, 711−716.
(28) Quail, J. C.; Rako, J. G.; Simon, H. J.; Deck, R. T. Optical Second-Harmonic Generation with Long-Range Surface Plasmons. *Phys. Rev. Lett.* **1983**, *50*, 1987−1989.
(29) Kauranen, M.; Zayats, A. V. Nonlinear plasmonics. *Nat. Photonics* **2012**, *6*, 737−748.
(30) Paarmann, A.; Razdolski, I.; Gewinner, S.; Schöllkopf, W.; Wolf, M. Effects of crystal anisotropy on optical phonon resonances in midinfrared second harmonic response of SiC. *Phys. Rev. B: Condens. Matter Mater. Phys.* **2016**, *94*, 134312.
(31) Schöllkopf, W.; Gewinner, S.; Junkes, H.; Paarmann, A.; von Helden, G.; Bluem, H.; Todd, A. M. M. The new IR and THz FEL facility at the Fritz Haber Institute in Berlin. *Proc. SPIE* **2015**, *9512*, 95121L.
(32) Berreman, D. W. Optics in Stratified and Anisotropic Media: 4 × 4-Matrix Formulation. *J. Opt. Soc. Am.* **1972**, *62*, 502.
(33) Yeh, P. Electromagnetic propagation in birefringent layered media. *J. Opt. Soc. Am.* **1979**, *69*, 742.
(34) Xu, W.; Wood, L. T.; Golding, T. D. Optical degeneracies in anisotropic layered media: Treatment of singularities in a 4 × 4 matrix formalism. *Phys. Rev. B: Condens. Matter Mater. Phys.* **2000**, *61*, 1740−1743.
(35) Paarmann, A.; Razdolski, I.; Melnikov, A.; Gewinner, S.; Schöllkopf, W.; Wolf, M. Second harmonic generation spectroscopy in the Reststrahl band of SiC using an infrared free-electron laser. *Appl. Phys. Lett.* **2015**, *107*, 081101.
(36) Engelbrecht, F.; Helbig, R. Effect of crystal anisotropy on the infrared reflectivity of 6H-SiC. *Phys. Rev. B: Condens. Matter Mater. Phys.* **1993**, *48*, 15698−15707.
(37) Bluet, J.; Chourou, K.; Anikin, M.; Madar, R. Weak phonon modes observation using infrared reflectivity for 4H, 6H and 15R polytypes. *Mater. Sci. Eng., B* **1999**, *61−62*, 212−216.
(38) Mayer, A.; Keilmann, F. Far-infrared nonlinear optics. I. $\chi^{(2)}$ near ionic resonance. *Phys. Rev. B: Condens. Matter Mater. Phys.* **1986**, *33*, 6954−6961.
(39) Caldwell, J. D.; Vurgaftman, I.; Tischler, J. G.; Glembocki, O. J.; Owrutsky, J. C.; Reinecke, T. L. Atomic-scale photonic hybrids for mid-infrared and terahertz nanophotonics. *Nat. Nanotechnol.* **2016**, *11*, 9−15.
(40) Neuner, B.; Korobkin, D.; Fietz, C.; Carole, D.; Ferro, G.; Shvets, G. Midinfrared Index Sensing of pL-Scale Analytes Based on Surface Phonon Polaritons in Silicon Carbide †. *J. Phys. Chem. C* **2010**, *114*, 7489−7491.
(41) De Leon, I.; Shi, Z.; Liapis, A. C.; Boyd, R. W. Measurement of the complex nonlinear optical response of a surface plasmon-polariton. *Opt. Lett.* **2014**, *39*, 2274.
(42) Hamm, P.; Zurek, M.; Mantele, W.; Meyer, M.; Scheer, H.; Zinth, W. Femtosecond infrared spectroscopy of reaction centers from Rhodobacter sphaeroides between 1000 and 1800 cm^{-1}. *Proc. Natl. Acad. Sci. U. S. A.* **1995**, *92*, 1826−1830.
(43) Zheng, G.; Chen, Y.; Bu, L.; Xu, L.; Su, W. Waveguide-coupled surface phonon resonance sensors with super-resolution in the mid-infrared region. *Opt. Lett.* **2016**, *41*, 1582.

DOI: 10.1021/acsphotonics.7b00118
ACS Photonics 2017, 4, 1048−1053